Accurate and Efficient Simulation and Design Using High-Order CFD Methods

Dr. Li Wang and Dr. W. Kyle Anderson

SimCenter: National Center for Computational Engineering
University of Tennessee at Chattanooga
Chattanooga, Tennessee, USA

July 9, 2014

Modern Techniques for Aerodynamic Analysis and Design
2014 CFD Summer School, Beijing, China, July 7-11, 2014

A Brief Overview

1. High-Order Discontinuous Galerkin Discretizations and Implicit Schemes
2. Multigrid Solution Acceleration Strategies
3. Adjoint-Based Mesh Adaptation and Shape Optimization
4. Simulation of Turbulence Using High-Order Discontinuous Galerkin Methods

Outline (Lecture 4)

1. Background & Motivation
2. Governing Equations and Subgrid Scale Model
3. Discretizations
    - Discontinuous Galerkin Discretizations
    - Implicit Time Integration Schemes
4. Surface Mesh Representation and Mesh Movement
5. Numerical Examples
6. Concluding Remarks

Outline (Lecture 4)

SimCenter
National Center for Computational Engineering

1. Background & Motivation
2. Governing Equations and Subgrid Scale Model
3. Discretizations
   - Discontinuous Galerkin Discretizations
   - Implicit Time Integration Schemes
4. Surface Mesh Representation and Mesh Movement
5. Numerical Examples
6. Concluding Remarks

Background & Motivation

- The turbulent world around us
- Current state-of-the-art in CFD and challenges
  1. Conventional second-order computational methods
  2. Difficulty encountered in accurate simulation of complex systems
- High-order accurate computational methods
  1. Reduction of mesh resolution while preserving accuracy
  2. Developed to tackle more complex problems
  3. Turbulent flow simulation
  4. Previous investigations on discontinuous Galerkin (DG) and stabilized upwind Petrov-Galerkin (SUPG) methods

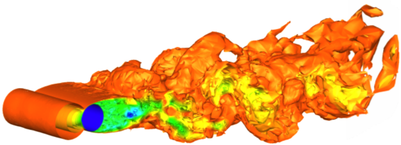

Flow around a circular cylinder (ILES, DG $p = 3$)

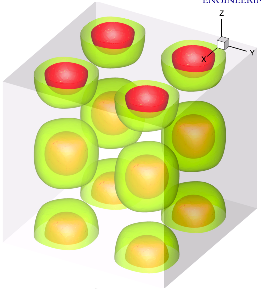

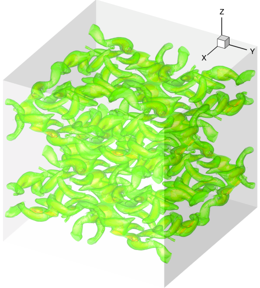

Taylor-Green vortex (DNS, DG $p = 4$)

- Simulations of Turbulence
  1. Direct Numerical Simulation (DNS)
     - ★ All time and length scales are resolved without any turbulence model.
     - ★ Stringent on grid sizes and time-step sizes
     - ★ Limitation for low Reynolds number flow and simple geometry
  2. Reynolds Averaged Navier-Stokes (RANS)
     - ★ All turbulence scales are modeled.
     - ★ Turbulence eddy viscosity can be determined through solving transport equations.
     - ★ Generally produce too much eddy viscosity and over-damp the unsteadiness
     - ★ Inadequate for resolving both periodic and the true dynamics
  3. Large Eddy Simulation (LES)
     - ★ Becoming a viable technique to predict unsteady turbulent flow
     - ★ Decompose a field-variable into resolved and subgrid components
     - ★ Directly resolve anisotropic large scales while modeling isotropic small scales
     - ★ Subgrid scale modeling, such as a wall-adapting local-eddy viscosity (WALE) model

- Simulations of Turbulence
  1. Direct Numerical Simulation (DNS)
     - ★ All time and length scales are resolved without any turbulence model.
     - ★ Stringent on grid sizes and time-step sizes
     - ★ Limitation for low Reynolds number flow and simple geometry
  2. Reynolds Averaged Navier-Stokes (RANS)
     - ★ All turbulence scales are modeled.
     - ★ Turbulence eddy viscosity can be determined through solving transport equations.
     - ★ Generally produce too much eddy viscosity and over-damp the unsteadiness
     - ★ Inadequate for resolving both periodic and the true dynamics
  3. Large Eddy Simulation (LES)
     - ★ Becoming a viable technique to predict unsteady turbulent flow
     - ★ Decompose a field-variable into resolved and subgrid components
     - ★ Directly resolve anisotropic large scales while modeling isotropic small scales
     - ★ Subgrid scale modeling, such as a wall-adapting local-eddy viscosity (WALE) model
- Objective: to investigate High-order Computational Methods for RANS and LES

Outline (Lecture 4)

SimCenter National Center for Computational Engineering

1. Background & Motivation
2. Governing Equations and Subgrid Scale Model
3. Discretizations
   - Discontinuous Galerkin Discretizations
   - Implicit Time Integration Schemes
4. Surface Mesh Representation and Mesh Movement
5. Numerical Examples
6. Concluding Remarks

Governing Equations (RANS)

- The compressible Reynolds Averaged Navier-Stokes (RANS) equations:

$$\frac{\partial \mathbf{U}(\mathbf{x},t)}{\partial t} + \nabla \cdot (\mathbf{F}_e(\mathbf{U}) - \mathbf{F}_v(\mathbf{U}, \nabla \mathbf{U})) = \mathbf{S}(\mathbf{U}, \nabla \mathbf{U})$$

- Fully coupled with the modified Spalart-Allmaras turbulence model
  Conservative flow vector: $\mathbf{U} = [\rho, \rho u, \rho v, \rho w, \rho E, \rho \tilde{v}]^T$
  The modified turbulence model equation:

$$\frac{\partial \rho \tilde{v}}{\partial t} + \nabla \cdot \left(\rho \mathbf{u} \tilde{v} - \frac{\mu}{\sigma}(1+\psi)\frac{\partial \tilde{v}}{\partial \mathbf{x}} \right) =$$

$$c_{b1}\tilde{S}\mu\psi - c_{w1}\rho f_w \left(\frac{\nu\psi}{d}\right)^2 + \frac{1}{\sigma}c_{b2}\rho\nabla\tilde{v}\cdot\nabla\tilde{v} - \frac{1}{\sigma}\nu(1+\psi)\nabla\rho\cdot\nabla\tilde{v}$$

  - ψ: auxiliary turbulence parameter
  - $\psi = f(\mathcal{X})$ and $\mathcal{X} = \frac{\tilde{v}}{\nu}$
  - d: distance to the nearest viscous wall

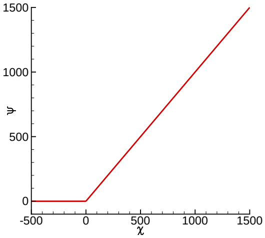

Governing Equations (LES)

- Filtering Operation in LES

$$\overline{\varphi}(\mathbf{x},t) = G(\bar{\Delta}) \star \varphi(\mathbf{x},t) \qquad \varphi''(\mathbf{x},t) = \varphi(\mathbf{x},t) - \overline{\varphi}(\mathbf{x},t)$$

- Filtered Compressible Navier-Stokes Equations
  - Conservation of mass

$$\frac{\partial \overline{\rho}}{\partial t} + \frac{\partial}{\partial x_j}(\overline{\rho}\tilde{u}_j) = 0$$

  - Conservation of momentum

$$\frac{\partial}{\partial t}(\overline{\rho}\tilde{u}_i) + \frac{\partial}{\partial x_j}(\overline{\rho}\tilde{u}_i\tilde{u}_j) + \frac{\partial}{\partial x_i}\overline{p} - \frac{\partial}{\partial x_j}\hat{\tau}_{ij} = -\frac{\partial}{\partial x_j}\tau_{ij}^{sgs}$$

  - Conservation of energy

$$\frac{\partial}{\partial t}(\overline{\rho}\hat{E}) + \frac{\partial}{\partial x_j}((\overline{\rho}\hat{E} + \overline{p})\tilde{u}_j) - \frac{\partial}{\partial x_j}(\tilde{u}_i\hat{\tau}_{ij}) + \frac{\partial}{\partial x_j}\hat{q}_j = -\frac{\partial}{\partial x_j}Q_j^{sgs}$$

  - Viscous stress tensor and heat flux vector

$$\hat{\tau}_{ij} = \frac{\mu}{Re}\left(\frac{\partial \tilde{u}_i}{\partial x_j} + \frac{\partial \tilde{u}_j}{\partial x_i} - \frac{2}{3}\delta_{ij}\frac{\partial \tilde{u}_k}{\partial x_k}\right), \quad \hat{q}_j = \frac{\gamma\mu}{P_r Re}\frac{\partial}{\partial x_j}\left(\hat{E} - \frac{1}{2}\tilde{u}_i\tilde{u}_i\right)$$

  - Equation of state for ideal gas

$$\overline{p} = (\gamma - 1)\overline{\rho}\left(\hat{E} - \frac{1}{2}\tilde{u}_j\tilde{u}_j\right)$$

Subgrid Scale Model

SimCenter National Center for Computational Engineering

- A closure requires subgrid scale modeling to τ_{ij}^{sgs} and Q_j^{sgs}.

$$\tau_{ij}^{sgs} = -\mu_T\left(\frac{\partial \tilde{u}_i}{\partial x_j} + \frac{\partial \tilde{u}_j}{\partial x_i} - \frac{2}{3}\delta_{ij}\frac{\partial \tilde{u}_k}{\partial x_k}\right) \qquad Q_j^{sgs} = \tilde{u}_i\tau_{ij}^{sgs} + \frac{\gamma\mu_T}{P_{r_T}}\frac{\partial}{\partial x_j}\left(\hat{E} - \frac{1}{2}\tilde{u}_i\tilde{u}_i\right)$$

Subgrid Scale Model

- A closure requires subgrid scale modeling to τ_{ij}^{sgs} and Q_j^{sgs}.

$$\tau_{ij}^{sgs} = -\mu_T\left(\frac{\partial \tilde{u}_i}{\partial x_j} + \frac{\partial \tilde{u}_j}{\partial x_i} - \frac{2}{3}\delta_{ij}\frac{\partial \tilde{u}_k}{\partial x_k}\right) \qquad Q_j^{sgs} = \tilde{u}_i \tau_{ij}^{sgs} + \frac{\gamma \mu_T}{P_{r_T}}\frac{\partial}{\partial x_j}\left(\hat{E} - \frac{1}{2}\tilde{u}_i\tilde{u}_i\right)$$

- Wall-Adapting Local-Eddy Viscosity (WALE) Model
  - Turbulent eddy viscosity, μ_T

$$\mu_T = \overline{\rho}(C_w\Delta)^2 \frac{(S_{ij}^d S_{ij}^d)^{3/2}}{(S_{ij}S_{ij})^{5/2} + (S_{ij}^d S_{ij}^d)^{5/4}}$$

  - Strain rate tensor, S_{ij}, and traceless symmetric tensor, S_{ij}^d

$$S_{ij} = \frac{1}{2}\left(\frac{\partial \tilde{u}_i}{\partial x_j} + \frac{\partial \tilde{u}_j}{\partial x_i}\right)$$

$$S_{ij}^d = \frac{1}{2}\left(\frac{\partial \tilde{u}_i}{\partial x_k}\frac{\partial \tilde{u}_k}{\partial x_j} + \frac{\partial \tilde{u}_j}{\partial x_k}\frac{\partial \tilde{u}_k}{\partial x_i}\right) - \frac{1}{3}\delta_{ij}\frac{\partial \tilde{u}_l}{\partial x_k}\frac{\partial \tilde{u}_k}{\partial x_l}$$

  - Based on the square of the velocity gradient tensor
  - Require local information that is easy to access for high-order methods

Discontinuous Galerkin Discretizations

- A weighted residual form for the RANS or the filtered LES-NS equations

$$\int_{\Omega_k} \phi_j \left[\frac{\partial \mathbf{U}_h(\mathbf{x},t)}{\partial t} + \nabla \cdot (\mathbf{F}_e(\mathbf{U}_h) - \mathbf{F}_v(\mathbf{U}_h, \nabla \mathbf{U}_h)) - \mathbf{S}(\mathbf{U}_h, \nabla \mathbf{U}_h) \right] d\Omega_k = 0.$$

- Integrate by parts and implemente of an explicit symmetric interior penalty (SIP) method

$$\begin{aligned}
&\int_{\Omega_k} \phi_j \frac{\partial \mathbf{U}_h}{\partial t} d\Omega_k - \int_{\Omega_k} \nabla \phi_j \cdot (\mathbf{F}_e(\mathbf{U}_h) - \mathbf{F}_v(\mathbf{U}_h, \nabla_h \mathbf{U}_h))\, d\Omega_k + \int_{\partial\Omega_k \setminus \partial\Omega} [[\underline{\phi_j}]] \mathbf{H}_c(\mathbf{U}_h^+, \mathbf{U}_h^-, \mathbf{n}) dS \\
&- \int_{\partial\Omega_k \setminus \partial\Omega} \{\mathbf{F}_v(\mathbf{U}_h, \nabla_h \mathbf{U}_h)\} \cdot [[\phi_j]] dS - \int_{\partial\Omega_k \setminus \partial\Omega} \{(\mathbf{G}_{i1} \frac{\partial \phi_j}{\partial \mathbf{x}_i}, \mathbf{G}_{i2} \frac{\partial \phi_j}{\partial \mathbf{x}_i}, \mathbf{G}_{i3} \frac{\partial \phi_j}{\partial \mathbf{x}_i})\} \cdot [[\mathbf{U}_h]] dS + \int_{\partial\Omega_k \setminus \partial\Omega} \vartheta \{\mathbf{G}\} [[\mathbf{U}_h]] \cdot [[\phi_j]] dS \\
&- \int_{\partial\Omega_k \cap \partial\Omega} \phi_j^+ \mathbf{F}_v^b(\mathbf{U}_b, \nabla_h \mathbf{U}_h^+) \cdot \mathbf{n} dS - \int_{\partial\Omega_k \cap \partial\Omega} (\mathbf{G}_{i1}(\mathbf{U}_b) \frac{\partial \phi_j^+}{\partial \mathbf{x}_i}, \mathbf{G}_{i2}(\mathbf{U}_b) \frac{\partial \phi_j^+}{\partial \mathbf{x}_i}, \mathbf{G}_{i3}(\mathbf{U}_b) \frac{\partial \phi_j^+}{\partial \mathbf{x}_i}) \cdot (\mathbf{U}_h^+ - \mathbf{U}_b) \mathbf{n} dS \\
&+ \int_{\partial\Omega_k \cap \partial\Omega} \vartheta \mathbf{G}(\mathbf{U}_b)(\mathbf{U}_h^+ - \mathbf{U}_b)\mathbf{n} \cdot \phi_j^+ \mathbf{n} dS + \int_{\partial\Omega_k \cap \partial\Omega} \phi_j \mathbf{F}_e(\mathbf{U}_b) \cdot \mathbf{n} dS - \int_{\Omega_k} \phi_j \mathbf{S}(\mathbf{U}_h, \nabla_h \mathbf{U}_h) = 0
\end{aligned}$$

where $\mathbf{G}_{1j} = \partial \mathbf{F}_v^x / \partial(\partial \mathbf{U} / \partial \mathbf{x}_j)$, $\mathbf{G}_{2j} = \partial \mathbf{F}_v^y / \partial(\partial \mathbf{U} / \partial \mathbf{x}_j)$ and $\mathbf{G}_{3j} = \partial \mathbf{F}_v^z / \partial(\partial \mathbf{U} / \partial \mathbf{x}_j)$

- Solution expansion and geometric mapping

$$\mathbf{U}_h = \sum_{i=1}^{M} \tilde{\mathbf{U}}_{h_i} \; \phi_i(\xi, \eta, \zeta) \qquad \mathbf{x}_k = \sum_{i=1}^{M} \tilde{\mathbf{x}}_{k_i} \phi_i(\xi, \eta, \zeta)$$

Implicit Time Integration Schemes

- The system of equations is expressed as

$$\mathbf{M}\frac{d\tilde{\mathbf{U}}_h}{dt} + \mathbf{R}(\tilde{\mathbf{U}}_h) = 0$$

- Implicit schemes are exclusively considered to avoid the stability limit.
  1. BDF2 (second-order accurate backward difference formula)

$$\mathbf{R}_e^{n+1}(\tilde{\mathbf{U}}_h^{n+1}) = \frac{\mathbf{M}}{\Delta t}(\tfrac{3}{2}\tilde{\mathbf{U}}_h^{n+1}) + \mathbf{R}(\tilde{\mathbf{U}}_h^{n+1}) - \frac{\mathbf{M}}{\Delta t}(2\tilde{\mathbf{U}}_h^{n} - \tfrac{1}{2}\tilde{\mathbf{U}}_h^{n-1}) = 0$$

  2. CN2 (second-order accurate Crank-Nicolson scheme)

$$\mathbf{R}_e^{n+1}(\tilde{\mathbf{U}}_h^{n+1}) = \frac{\mathbf{M}}{\Delta t}\tilde{\mathbf{U}}_h^{n+1} + \tfrac{1}{2}\mathbf{R}(\tilde{\mathbf{U}}_h^{n+1}) - \frac{\mathbf{M}}{\Delta t}(\tilde{\mathbf{U}}_h^{n} - \tfrac{1}{2}\mathbf{R}(\tilde{\mathbf{U}}_h^{n})) = 0$$

  3. IRK4 (fourth-order accurate implicit Runge-Kutta scheme)

$$\mathbf{R}_e^{n+1}(\tilde{\mathbf{U}}_h^{(s),n+1}) = \frac{\mathbf{M}}{\Delta t}\tilde{\mathbf{U}}_h^{(s),n+1} + a_{ss}\mathbf{R}(\tilde{\mathbf{U}}_h^{(s),n+1}) - \left(\frac{\mathbf{M}}{\Delta t}\tilde{\mathbf{U}}_h^{n} - \sum_{j=1}^{s-1} a_{sj}\mathbf{R}(\tilde{\mathbf{U}}_h^{(j),n+1})\right) = 0$$

- Solved by an approximate Newton method
  - ILU(k) preconditioned GMRES algorithm [Saad and Schultz 1996]
  - p-multigrid method driven by a linearized element Gauss-Seidel smoother [Wang and Mavriplis 2007]
- For steady state problems, a local time-stepping method is used to alleviate initial transient effects.

Outline (Lecture 4)

1. Background & Motivation
2. Governing Equations and Subgrid Scale Model
3. Discretizations
   - Discontinuous Galerkin Discretizations
   - Implicit Time Integration Schemes
4. Surface Mesh Representation and Mesh Movement
5. Numerical Examples
6. Concluding Remarks

Surface Mesh Representation and Mesh Movement

- High-fidelity surface definition is required for high-order methods.
- Incorporate CAPRI [Haimes and Follen 1998] to allow communication with CAD software
- Determine the coordinates of additional surface quadrature points

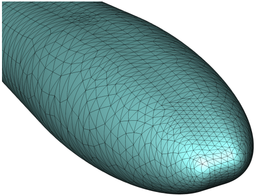

3D analytical body

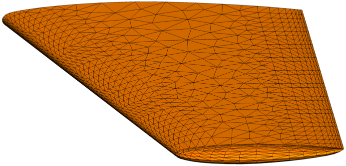

ONERA M6 wing

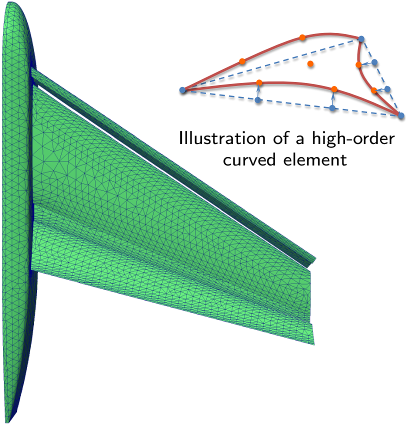

High-order surface representation for Trap wing

Illustration of a high-order curved element

Surface Mesh Representation and Mesh Movement

- Mesh movement is required for viscous meshes.

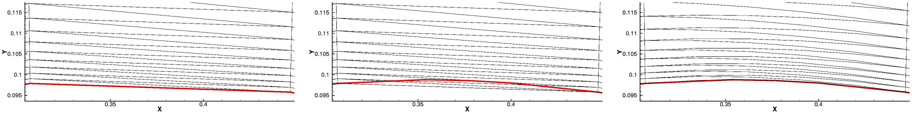

- Interior mesh deformations are determined by solving the linear elasticity equations:

$$\frac{\partial}{\partial x}\left[d_{11}\frac{\partial \delta_x}{\partial x}+d_{12}\frac{\partial \delta_y}{\partial y}+d_{13}\frac{\partial \delta_z}{\partial z}\right]+\frac{\partial}{\partial y}\left[d_{44}\left(\frac{\partial \delta_x}{\partial y}+\frac{\partial \delta_y}{\partial x}\right)\right]+\frac{\partial}{\partial z}\left[d_{66}\left(\frac{\partial \delta_x}{\partial z}+\frac{\partial \delta_z}{\partial x}\right)\right]=0$$

$$\frac{\partial}{\partial x}\left[d_{44}\left(\frac{\partial \delta_x}{\partial y}+\frac{\partial \delta_y}{\partial x}\right)\right]+\frac{\partial}{\partial y}\left[d_{21}\frac{\partial \delta_x}{\partial x}+d_{22}\frac{\partial \delta_y}{\partial y}+d_{23}\frac{\partial \delta_z}{\partial z}\right]+\frac{\partial}{\partial z}\left[d_{55}\left(\frac{\partial \delta_y}{\partial z}+\frac{\partial \delta_z}{\partial y}\right)\right]=0$$

$$\frac{\partial}{\partial x}\left[d_{66}\left(\frac{\partial \delta_x}{\partial z}+\frac{\partial \delta_z}{\partial x}\right)\right]+\frac{\partial}{\partial y}\left[d_{55}\left(\frac{\partial \delta_y}{\partial z}+\frac{\partial \delta_z}{\partial y}\right)\right]+\frac{\partial}{\partial z}\left[d_{31}\frac{\partial \delta_x}{\partial x}+d_{32}\frac{\partial \delta_y}{\partial y}+d_{33}\frac{\partial \delta_z}{\partial z}\right]=0$$

$$d_{11}=d_{22}=d_{33}=\frac{E(1-\upsilon)}{(1+\upsilon)(1-2\upsilon)}$$

$$d_{12}=d_{13}=d_{21}=d_{23}=d_{31}=d_{32}=\frac{E\upsilon}{(1+\upsilon)(1-2\upsilon)}$$

$$d_{44}=d_{55}=d_{66}=\frac{E}{2(1+\upsilon)}$$

  - $\delta=(\delta_x,\delta_y,\delta_z)^T$ represents the perturbations at mesh points and quadrature points.
  - Dirichlet boundary conditions are realized progressively in a sequence of small steps.
  - Solved by ILU(k) preconditioned GMRES algorithm.

1. 2D turbulent NACA-0012 airfoil
2. Assessment of accuracy and efficiency for LES
3. LES computation for flow over a bluff-body square cylinder
4. LES computation for flow over a three-dimensional NACA-0012 airfoil

Turbulent 2D NACA-0012 Airfoil

- $Re = 6{,}000{,}000, M_\infty = 0.15, \alpha = 0^\circ$
- Study on the effect of wall coordinate (y^+) and viscous stretching factor (β)
- Use of the DG $p = 2, 3$ and 4 discretizations with the modified SA model

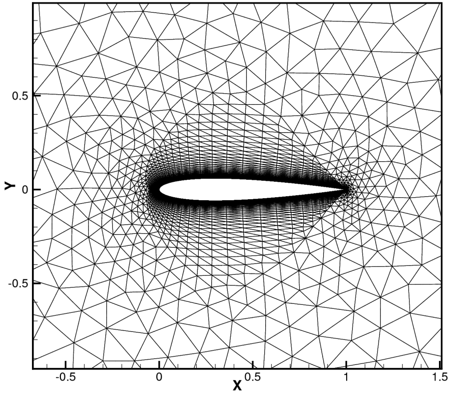

Computational mesh (containing 9671 triangular elements) with $y^+ = 1$

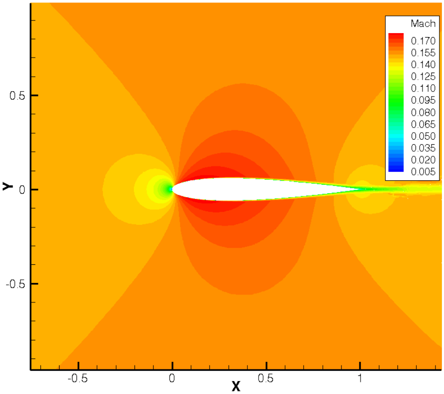

Contours of Mach number solution ($p = 4$)

Turbulent 2D NACA-0012 Airfoil

- Effect of wall coordinate y^+ ($\beta = 1.15$)

y^+	1	5	10	15
nElem	9671	8573	7775	7269

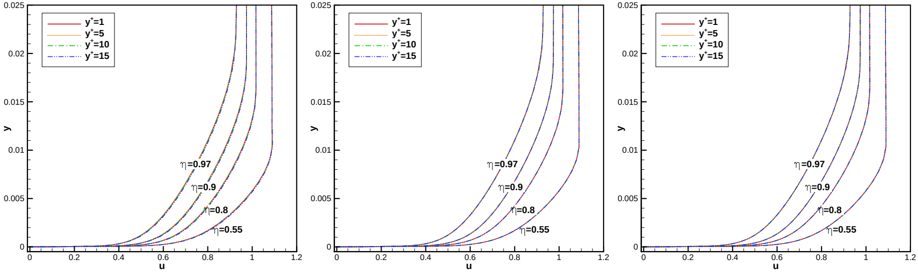

$p = 2$ $p = 3$ $p = 4$

Solution profiles for meshes with y^+ of 1, 5, 10 and 15 using different DG schemes from $p = 2$ to $p = 4$

Turbulent 2D NACA-0012 Airfoil

- Effect of wall coordinate y^+ ($\beta = 1.15$)

y^+	1	5	10	15
nElem	9671	8573	7775	7269

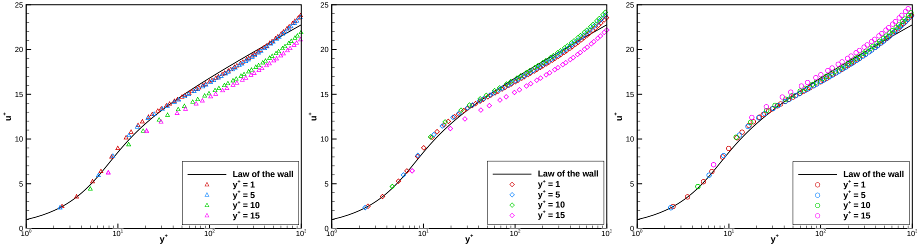

$p = 2$ $p = 3$ $p = 4$

Profiles of law-of-the-wall for meshes with y^+ of 1, 5, 10 and 15 using different DG schemes from $p = 2$ to $p = 4$

- Effect of viscous stretching factor β ($y^+ = 5$)

β	1.15	1.2	1.3	1.4
nElem	8573	6965	5409	4581

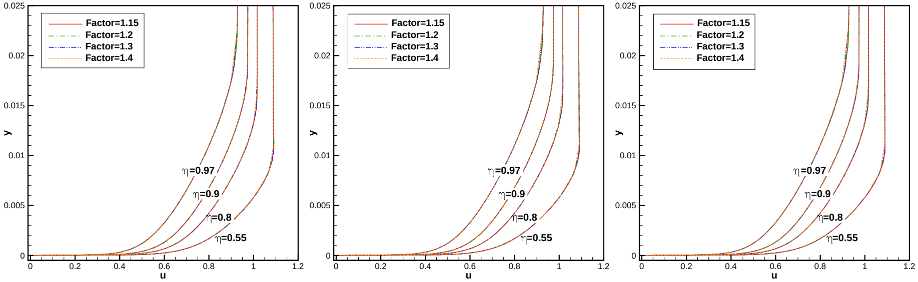

$p = 2$ $p = 3$ $p = 4$

Solution profiles for meshes with β of 1.15, 1.2, 1.3 and 1.4 using different DG schemes from $p = 2$ to $p = 4$

- Effect of viscous stretching factor β ($y^+ = 5$)

β	1.15	1.2	1.3	1.4
nElem	8573	6965	5409	4581

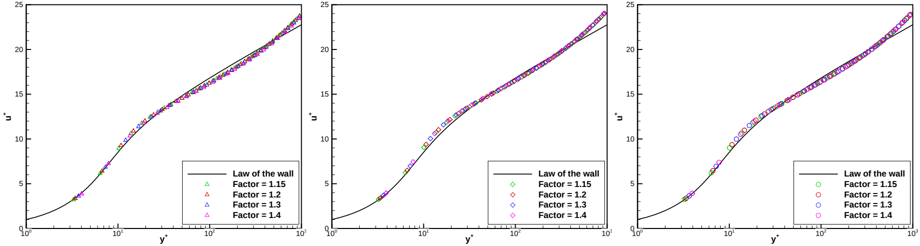

$p = 2$ $p = 3$ $p = 4$

Profiles of law-of-the-wall for meshes with β of 1.15, 1.2, 1.3 and 1.4 using different DG schemes from $p = 2$ to $p = 4$

Assessment of Accuracy and Efficiency for LES

- Assessed by means of the Method of Manufactured Solution (MMS)
- Performed using the LES-WALE equations while excluding the time-derivative term
- Manufactured solution:

$$\{\rho, u, v, \rho E\}_{ex}^{T} = \left\{ \begin{array}{c} \rho_0(1+\sin(\pi x)\cos(\pi x)\sin(\pi y)\cos(\pi y)) \\ u_0(1+\sin(k\pi x)\cos(k\pi x)\sin(k\pi y)\cos(k\pi y)) \\ v_0(1+\sin(k\pi x)\cos(k\pi x)\sin(k\pi y)\cos(k\pi y)) \\ E_{t_0}(1+\sin(\pi x)\sin(\pi x)\sin(\pi y)\sin(\pi y)) \end{array} \right\}$$

- Parameter setting: $(\rho_0, u_0, v_0, E_{t_0}) = (1, 2.5, 1.5, 10)$, $k = 2$ and $Re = 20000$
- L_2-norm error:

$$||\mathbf{U}_{ex} - \mathbf{U}_h||_{L_2} = \sqrt{\frac{\int_\Omega (\mathbf{U}_{ex} - \mathbf{U}_h)^2 d\Omega}{\int_\Omega d\Omega}}$$

- Various orders of discontinuous Galerkin schemes ranging from $P = 1$ to $P = 3$
- A sequence of 4 grids of $N = 800$, 3200, 12800 and 51200 triangular elements in a square domain of dimension 1×1

- Exact solutions in the MMS

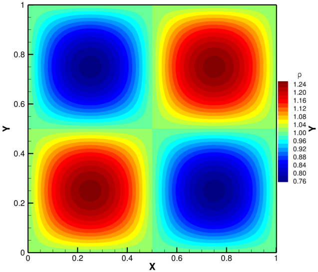

Density, ρ

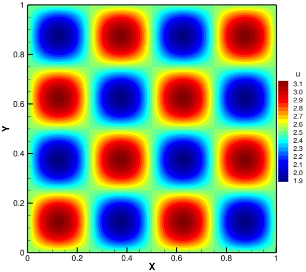

Streamwise velocity, u

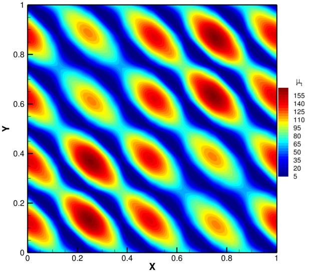

Turbulent eddy viscosity, μ_T

Order-of-Accuracy

- Solution error versus mesh spacing, $h = 1/\sqrt{N}$

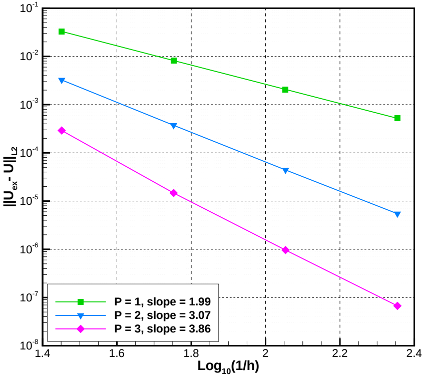

  - Optimal order of accuracy ($\sim h^{P+1}$) is achieved.
  - Saving in mesh density can be achieved through the use of a higher-order scheme.

Order-of-Accuracy

- Solution error versus mesh spacing, $h = 1/\sqrt{N}$

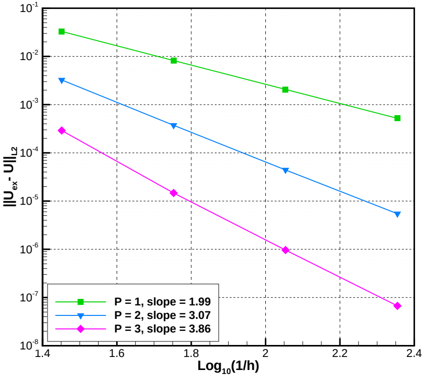

- Optimal order of accuracy ($\sim h^{P+1}$) is achieved.
- Saving in mesh density can be achieved through the use of a higher-order scheme.
  - Example: to achieve an error level of 10^{-4}:

Order	$P = 1$	$P = 2$	$P = 3$
N	288,403	7,585	1,318
Factor	1	38	218

Computational Efficiency

- *P*-multigrid algorithm with a linearized element Gauss-Seidel smoother
- Solution error versus CPU time

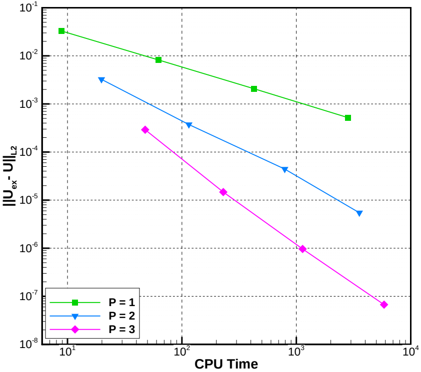

- A higher-order scheme outerperforms a lower-order counterpart.

Computational Efficiency

- *P*-multigrid algorithm with a linearized element Gauss-Seidel smoother
- Solution error versus CPU time

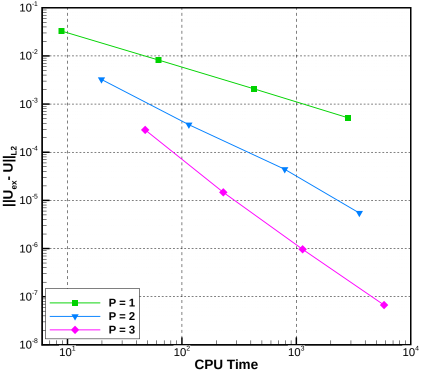

- A higher-order scheme outerperforms a lower-order counterpart.
  - ★ Example: to achieve an error level of 10^{-4}:

Order	$P = 1$	$P = 2$	$P = 3$
CPU Time (s)	23030	375	82
Speedup	1	61	280

Turbulent Flow Over a Bluff-Body Square Cylinder

SimCenter National Center for Computational Engineering

- $M_\infty = 0.1$ and $Re = 22,000$
- Two dimensional in the mean
- Various orders of spatial schemes: $P = 1$ to $P = 3$
- Temporal schemes: BDF2, CN2 ($\Delta t = 0.001$) and IRK4 ($\Delta t = 0.002$)
- Computational domain: $[-10D, 30D] \times [-10D, 10D]$ in x and y directions

Turbulent Flow Over a Bluff-Body Square Cylinder

- $M_\infty = 0.1$ and $Re = 22,000$
- Two dimensional in the mean
- Various orders of spatial schemes: $P = 1$ to $P = 3$
- Temporal schemes: BDF2, CN2 ($\Delta t = 0.001$) and IRK4 ($\Delta t = 0.002$)
- Computational domain: $[-10D, 30D] \times [-10D, 10D]$ in x and y directions

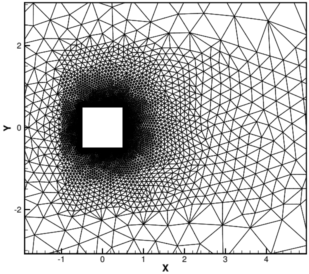

Computational mesh ($N = 41,816$ and $D = 1$)

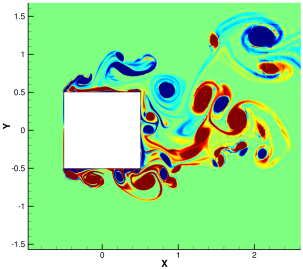

Instantaneous z-vorticity ($P = 3$)

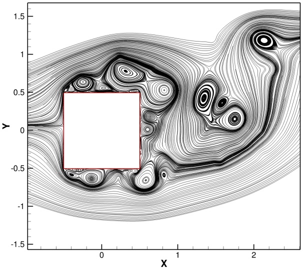

Streamlines ($P = 3$)

Effect on Temporal Accuracy

- Turbulent boundary-layer statistics studies
- Fix the spatial scheme as $P = 3$ to eliminate the effect of spatial error
- Comparison among the BDF2, CN2 and IRK4 schemes with Lyn's experiments [Lyn and Rodi 1995]

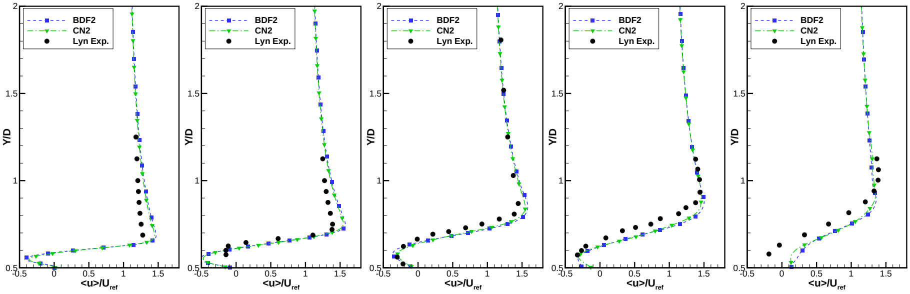

$x/D = -0.375$ $x/D = -0.25$ $x/D = 0$ $x/D = 0.25$ $x/D = 0.5$

Effect on Temporal Accuracy

- Turbulent boundary-layer statistics studies
- Fix the spatial scheme as $P = 3$ to eliminate the effect of spatial error
- Comparison among the BDF2, CN2 and IRK4 schemes with Lyn's experiments [Lyn and Rodi 1995]

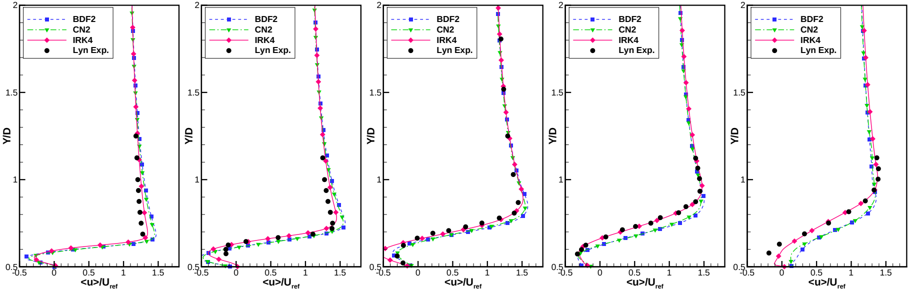

$x/D = -0.375$ $x/D = -0.25$ $x/D = 0$ $x/D = 0.25$ $x/D = 0.5$

Effect on Spatial Accuracy

- Turbulent boundary-layer statistics studies
- Fix the temporal scheme (IRK4) to eliminate the effect of temporal error
- Comparison among the second, third and fourth-order DG schemes with Lyn's experiments [Lyn and Rodi 1995]

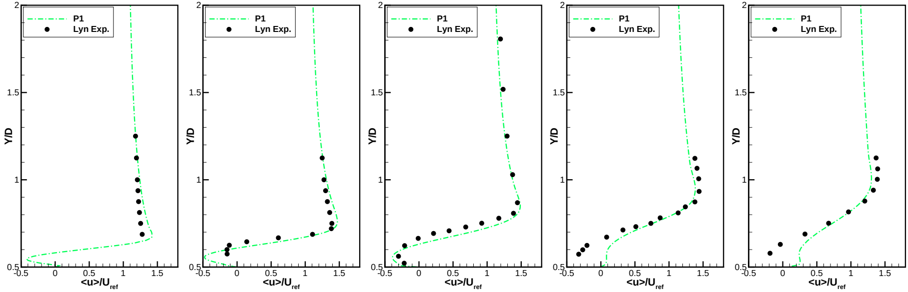

$x/D = -0.375$ $x/D = -0.25$ $x/D = 0$ $x/D = 0.25$ $x/D = 0.5$

Effect on Spatial Accuracy

- Turbulent boundary-layer statistics studies
- Fix the temporal scheme (IRK4) to eliminate the effect of temporal error
- Comparison among the second, third and fourth-order DG schemes with Lyn's experiments [Lyn and Rodi 1995]

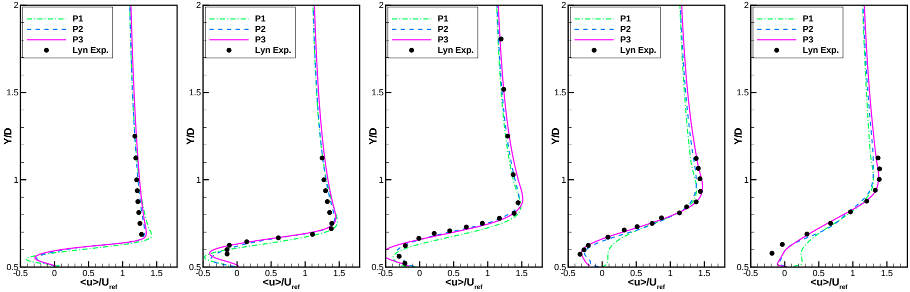

$x/D = -0.375$ $x/D = -0.25$ $x/D = 0$ $x/D = 0.25$ $x/D = 0.5$

Effect on Spatial Accuracy

- Statistical study on the wake structures
- Comparison among the second, third and fourth-order DG schemes with experimental data from Lyn [Lyn and Rodi 1995] and Durao [Durao and Heitor 1958]

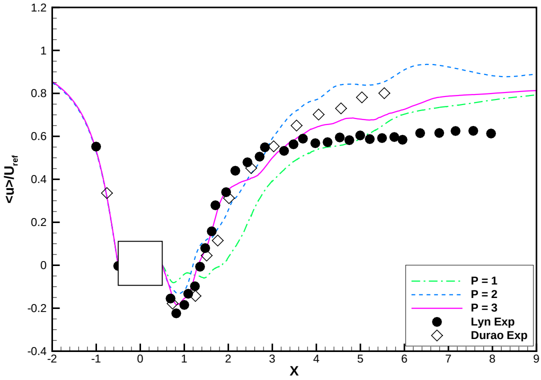

Turbulent Flow over a Three-Dimensional NACA-0012 Airfoil

- $M_\infty = 0.1$, $Re = 50,000$, AOA$=5^\circ$ and 8°
- Second and third-order discontinuous Galerkin schemes
- Time-integration: the BDF2 scheme with $\Delta t = 0.001$

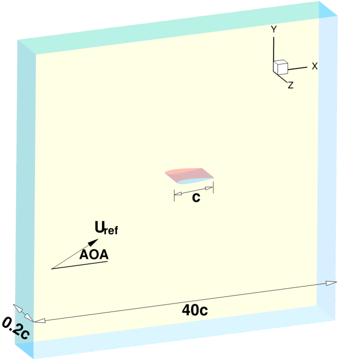

Geometry definition

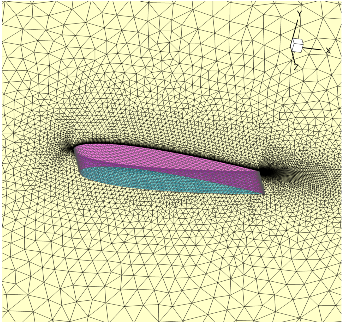

Computational mesh ($N = 925,200$ unstructured tetrahedrons)

- Spanwise: 16 two-dimensional planes with a constant interval
- Wall spacing $y^+ \approx 1$, streamwise $x^+ \approx 60$ and spanwise $z^+ \approx 40$

Flow Field Description

- Instantaneous flow field, AOA=5° and 8°
- Contours of entropy ($P = 2$)

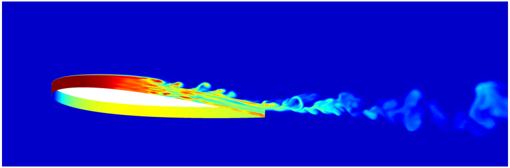

AOA=5°

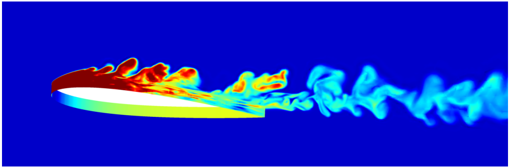

AOA=8°

Flow Field Description

- Instantaneous flow field, AOA=5° and 8°
- Isosurfaces of Q-criterion ($P = 2$) of values ranging from 1 to 20, colored by vorticity magnitude; $Q = -\frac{1}{2}\left(S_{ij}S_{ij} - \Omega_{ij}\Omega_{ij}\right)$.

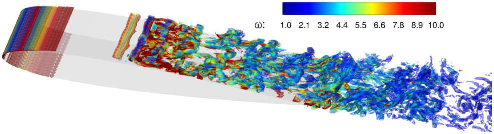

AOA=5°

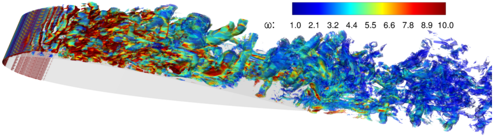

AOA=8°

Study on Case of AOA=8°

- Turbulent boundary-layer statistics and wake
- Obtain combined time-and-spanwise averaged (i.e. mean) solutions

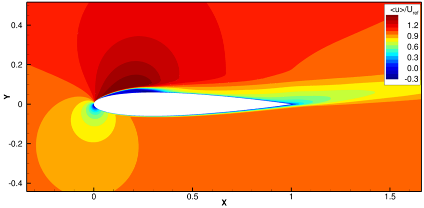

$< u >$

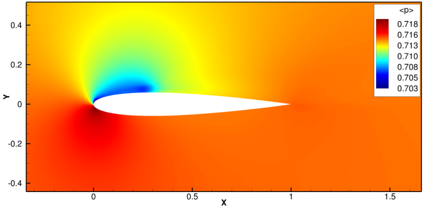

$< p >$

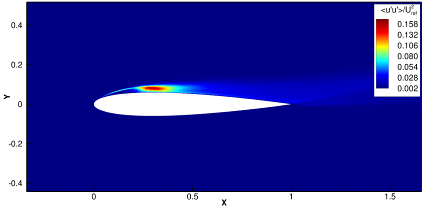

$< u'u' >$

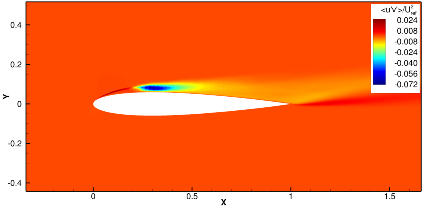

$< u'v' >$

Study on Case of AOA=8°

- Time-and-spanwise averaged surface pressures
- Comparison with the DNS solution [Lehmkuhl et al. 2011]

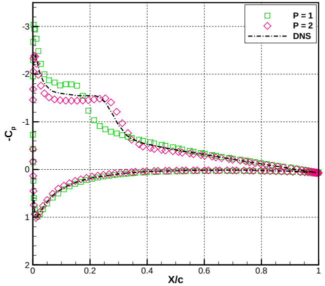

Study on Case of AOA=8°

- Time-and-spanwise averaged surface pressures
- Comparison with the DNS solution [Lehmkuhl et al. 2011]

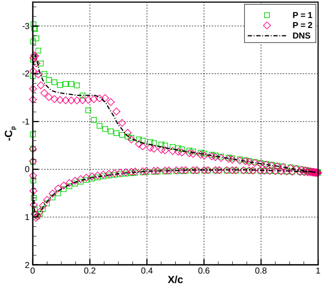

- Aerodynamic properties

Computation	x_{sep}/c	x_{reatt}/c
DNS	0.0241	0.320
LES-WALE DG $P = 1$	0.0273	0.231
LES-WALE DG $P = 2$	0.0281	0.341

Mean Velocity Profiles

- Combined time-and-spanwise averaged (i.e. mean) solutions
- Various stations on the airfoil suction side and wake
- Comparison with the DNS solution [Lehmkuhl et al. 2011]

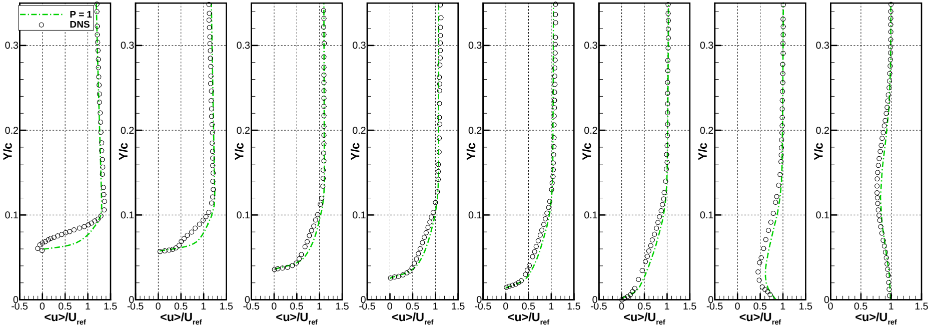

$x/c = 0.3$ $x/c = 0.4$ $x/c = 0.7$ $x/c = 0.8$ $x/c = 0.9$ $x/c = 1.0$ $x/c = 1.2$ $x/c = 2.0$

Mean Velocity Profiles

- Combined time-and-spanwise averaged (i.e. mean) solutions
- Various stations on the airfoil suction side and wake
- Comparison with the DNS solution [Lehmkuhl et al. 2011]

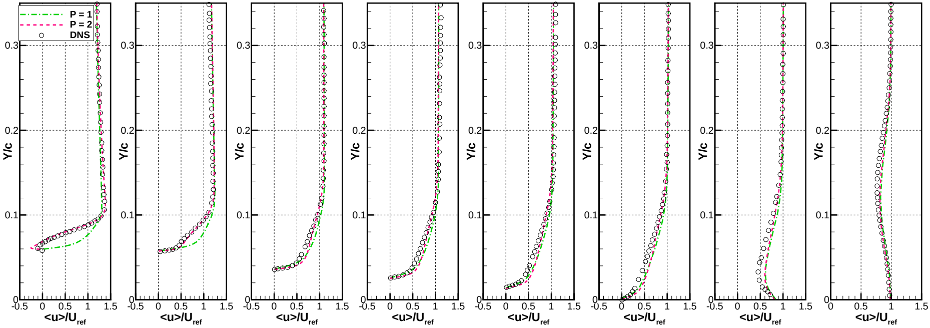

$x/c = 0.3$ $x/c = 0.4$ $x/c = 0.7$ $x/c = 0.8$ $x/c = 0.9$ $x/c = 1.0$ $x/c = 1.2$ $x/c = 2.0$

- Combined time-and-spanwise averaged (i.e. mean) solutions
- Various stations on the airfoil suction side and wake
- Comparison with the DNS solution [Lehmkuhl et al. 2011]
- Profiles of normalized streamwise Reynolds stress $< u'u' > /U_{ref}^2$

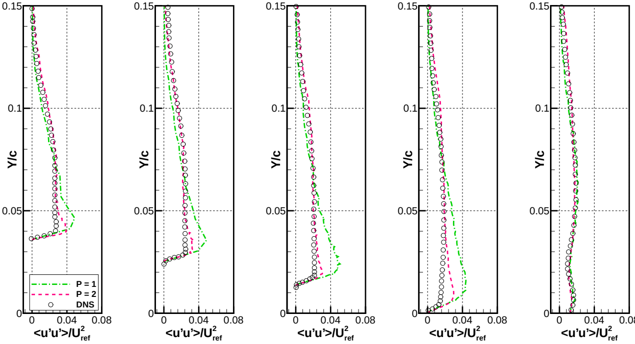

$x/c = 0.7$ $x/c = 0.8$ $x/c = 0.9$ $x/c = 1.0$ $x/c = 1.2$

Turbulent Statistics

- Combined time-and-spanwise averaged (i.e. mean) solutions
- Various stations on the airfoil suction side and wake
- Comparison with the DNS solution [Lehmkuhl et al. 2011]
- Profiles of normalized shear stress $< u'v' > / U_{ref}^2$

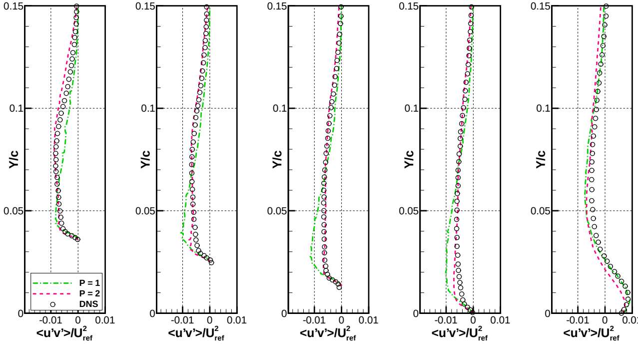

$x/c = 0.7$ $x/c = 0.8$ $x/c = 0.9$ $x/c = 1.0$ $x/c = 1.2$

Instantaneous Turbulent Eddy Viscosity

- Comparison of μ_T resolved in the second and third-order DG schemes
- Contours at $z = 0$ plane

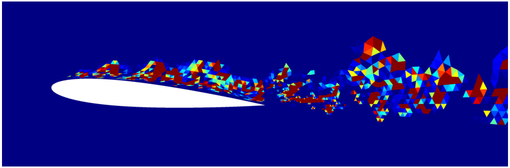

$P = 1$

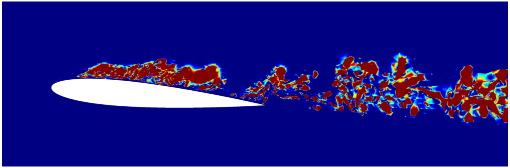

$P = 2$

Concluding Remarks

- A consistent high-order discretization to the modified SA turbulence model performs very well regarding accuracy and robustness.
- The conventional setting for the wall spacing and stretching factor can be less stringent when high-order methods are used for RANS.
  - Attached flow and $p \geq 2$: wall coordinate $y^+ \approx 5$ or 10, stretching factor $\beta \approx 1.4$
- Geometry curvatures must be properly represented to guarantee the solution accuracy.
  - High-order representation for surface geometry
  - Determination of the physical positions for surface quadrature points

Concluding Remarks

SimCenter
National Center for Computational Engineering

- A high-order discontinuous Galerkin FE method is developed for large-eddy simulation (LES).
  - The wall-adapting local-eddy viscosity (WALE) model is investigated.
  - Turbulent eddy viscosity can be explicitly computed for subgrid scale terms.
  - Compact stencil is maintained and robustness is improved.
- Order-of-accuracy and computational efficiency are assessed by means of MMS.
  - Optimal error convergence is attained for the LES-WALE equations.
  - Higher-order DG schemes outperform a lower-order counterpart to achieve a given error level.
- Higher-order schemes are capable of accurately capturing both mean flow quantities and turbulent statistics.
  - Turbulent fluctuations are often several orders of magnitude smaller than the mean flow.
  - Difficulty is encountered for resolving the smaller scales using a lower-order scheme.

References

L. Wang, W. K. Anderson, T. Erwin and S. Kapadia, Discontinuous Galerkin and Petrov Galerkin Methods for Compressible Viscous Flows, Computers and Fluids, 100, 13-29, 2014.

J. Erwin, W. K. Anderson, L. Wang and S. Kapadia, High-Order Finite-Element Method for Three-Dimensional Turbulent Navier-Stokes, AIAA Paper 2013-2571, 21st AIAA Computational Fluid Dynamics Conference, 2013.

L. Wang, W. K. Anderson, T. Erwin, S. Kapadia, High-order methods for solutions of three-dimensional turbulent flows, AIAA Paper 2013-0856, 2013.

F. Ducros, F. Nicoud, T. Poinsot, Wall-adapting local eddy-viscosity models for simulations in complex geometries, In 6th Numerical Methods for Fluid Dynamics Conference (1998).

B. Verman, B. Geurts, H. Kuerten, A priori tests of large eddy simulatin of the compressible plane mixing layer, J. Eng. Math. 29 (1995) 299-327.

E. Garnier, Dr. N. Adams, P. Sagaut, Large Eddy Simulation for Compressible Flows, ISBN: 978-90-481-2818-1, Springer, 2009.